Real-time imaging of single nerve cell apoptosis in retinal neurodegeneration

M. Francesca Cordeiro*†, Li Guo*, Vy Luong‡, Glen Harding‡, Wei Wang‡, Helen E. Jones‡, Stephen E. Moss§, Adam M. Sillito‡, and Frederick W. Fitzke‡

*Department of Pathology and Glaucoma and Optic Nerve Head Research Group, and Departments of ‡Visual Sciences and §Cell Biology, Institute of Ophthalmology, University College London, Bath Street, London EC1V 9EL, United Kingdom

Communicated by Alfred Sommer, Johns Hopkins University, Baltimore, MD, July 28, 2004 (received for review June 1, 2004)

Apoptotic nerve cell death is implicated in the pathogenesis of several devastating neurodegenerative conditions, including glaucoma and Alzheimer's and Parkinson's diseases. We have devised a noninvasive real-time imaging technique using confocal laser-scanning ophthalmoscopy to visualize single nerve cell apoptosis *in vivo*, which allows longitudinal study of disease processes that has not previously been possible. Our method utilizes the unique optical properties of the eye, which allow direct microscopic observation of nerve cells in the retina. We have been able to image changes occurring in nerve cell apoptosis over hours, days, and months and show that effects depend on the magnitude of the initial apoptotic inducer in several models of neurodegenerative disease in rat and primate. This technology enables the direct observation of single nerve cell apoptosis in experimental neurodegeneration, providing the opportunity for detailed investigation of fundamental disease mechanisms and the evaluation of interventions with potential clinical applications, together with the possibility of taking this method through to patients.

Apoptosis is an orchestrated form of cell "death by suicide." It is essential in both the development and normal maintenance of tissue function. It is also implicated in the pathology of a number of severe neurodegenerative disorders such as glaucoma, motor neuron, and Alzheimer's, Parkinson's, and Huntington's diseases (1). There is evidence that a similar pathogenesis may contribute to neurodegenerative processes in these conditions (2), and that the extent of nerve cell loss is correlated with functional deficit (3–6). If we could directly visualize this process, it would facilitate a much more precise diagnosis and critically enable accurate tracking of the disease state and the action of therapy. However, until now, it has not been possible to detect nerve cell apoptosis *in vivo* (1, 7–10).

Annexin 5 is a protein that, in the presence of Ca^{2+}, has a high affinity for phosphatidylserine (PS), an anionic phospholipid that is enriched in the inner leaflet of plasma membranes. The externalization of PS from the inner leaflet to the outer layer of the cell membrane is an invariant early feature in the apoptotic process that occurs before DNA fragmentation and nuclear condensation. Because of its properties, FITC-annexin 5 has become widely used in the cytological detection of cells undergoing apoptosis (11). More recently, annexin 5 has been shown to be effective in the identification of apoptosis *in vivo* by using radiological and macroscopic fluorescent techniques (7, 8, 10, 12, 13).

However, existing *in vivo* techniques using annexin 5 either have been unable to resolve the process to a single cellular level (7–9) or require an invasive method performed under terminal anesthesia (10). Imaging the eye, compared with the rest of the body, offers a unique opportunity because of the presence of clear optical media allowing direct visualization of labeled disease processes as they occur. This means images may be acquired repeatedly in a noninvasive manner.

We have devised and have used a method that allows us to track neuronal apoptotic changes over time. We have explored it in three rat models that generate differing patterns of apoptotic retinal ganglion cell (RGC) death, as well as in a primate model that clearly underlines the power of the technique and the ability to transfer it to the patient. This technique is an important advance in our ability to investigate and monitor disease mechanisms in experimental neurodegeneration.

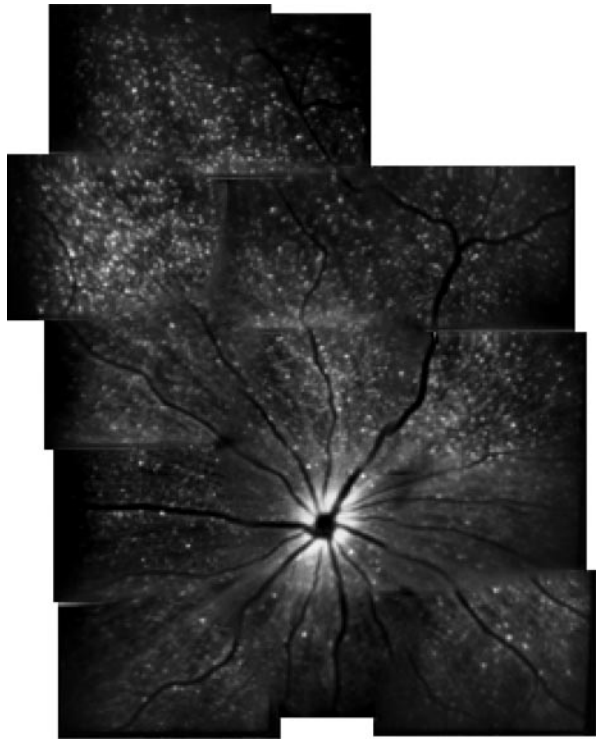

Fig. 1. Visualization of nerve cell apoptosis. We demonstrated that RGC apoptosis could be detected *in vivo* by using a modified cLSO with an argon laser (488 nm) for illumination and a wide band-pass filter with short-wavelength cutoff of a 521-nm filter and intravitreal Alexa Fluor 488 fluorescent-labeled annexin 5. We investigated rat models of glaucoma, optic nerve transection, and a model using SSP. This animal's eye was treated with intravitreal SSP (0.5 μg). The retinal montage, constructed from images captured at the same time point (90 min), shows extensive and widespread RGC apoptosis (white spots, annexin 5-positive apoptotic cells).

Materials and Methods

Animal Models. All procedures complied with local and national regulations and were performed under general anesthesia. Adult Dark Agouti rats, 150–200 g, were used in all rat experiments.

Abbreviations: cLSO, confocal laser scanning ophthalmoscope; DiAsp, (4- (4-(didecylamino) styryl)-*N*-methylpyridinium iodide); IOP, intraocular pressure; OHT, ocular hypertension; RGC, retinal ganglion cell; SSP, staurosporine.

†To whom correspondence should be addressed. E-mail: m.cordeiro@ucl.ac.uk.

www.pnas.org/cgi/doi/10.1073/pnas.0405479101

Ocular hypertension (OHT). Eighteen rats underwent surgery to elevate intraocular pressure (IOP) by injection of hypertonic saline solution (1.80 M) into two episcleral veins, as described (14). Contralateral unoperated eyes acted as controls. The IOP of both eyes in each rat was measured at regular intervals by using a Tonopen XL (Medtronic Solan, Jacksonville, FL). For each animal, the IOP was recorded, and a graph of IOP elevation (difference between IOP in operated and control eyes) over time was constructed, from which the ΔIOP integral was calculated from the area under the curve. Animals were imaged at 2, 3, 4, 8, 12, and 16 weeks, with at least three animals at each time point being killed for histology soon after imaging.

Optic nerve transection. The retrobulbar optic nerve of 12 rats was exposed, and the nerve fibers were completely transected at a distance of 2–3 mm from the globe, with care not to damage the nerve vasculature and optic nerve blood supply, as described (15). The injury was unilateral, with the other eye serving as control. Animals were imaged at 8 h and at 3, 7, and 12 days and were killed for histology soon after ($n = 3$ per time point).

Staurosporine (SSP)-induced apoptosis. Fifteen Dark Agousti rats received different doses of intravitreal SSP (0, 0.125, 0.25, 0.5, and 1.0 μg in 5 μl of PBS; both from Sigma–Aldrich). Animals were imaged immediately and up to 6 h, after which they were killed for histology ($n = 3$ per dose).

Analysis of two macaque monkeys was performed while animals were anesthetized [sufentanil 4 μg/kg per hour or halothane (0.1–0.4%) in 70% N_2O/30% O_2] and paralyzed (0.1 mg/kg per hour vecuronium bromide) by using published methods (16). After intravitreal SSP administration (2.5, 5.0, 7.5, and 10 μg in 50 μl), animals were imaged for at least 6 h.

Imaging with Alexa Fluor 488-Labeled Annexin 5. The imaging method is based on a prototype Zeiss confocal laser scanning ophthalmoscope (cLSO) with specialized imaging software to compensate for eye movements and improve the signal-to-noise ratio (17, 18). Briefly, the animal was positioned before the cLSO so that the interior of the eye was imaged. An Argon laser wavelength of 488 nm was focused into a small spot and scanned across the retina by a pair of mirrors to excite the administered annexin 5-bound fluorophore. The resulting fluorescence was optically focused onto a confocal aperture that had the effect of excluding unwanted fluorescence in planes above or below the depth plane of interest. After passing back through the pair of scanning mirrors, the fluorescence was detected by a solid-state

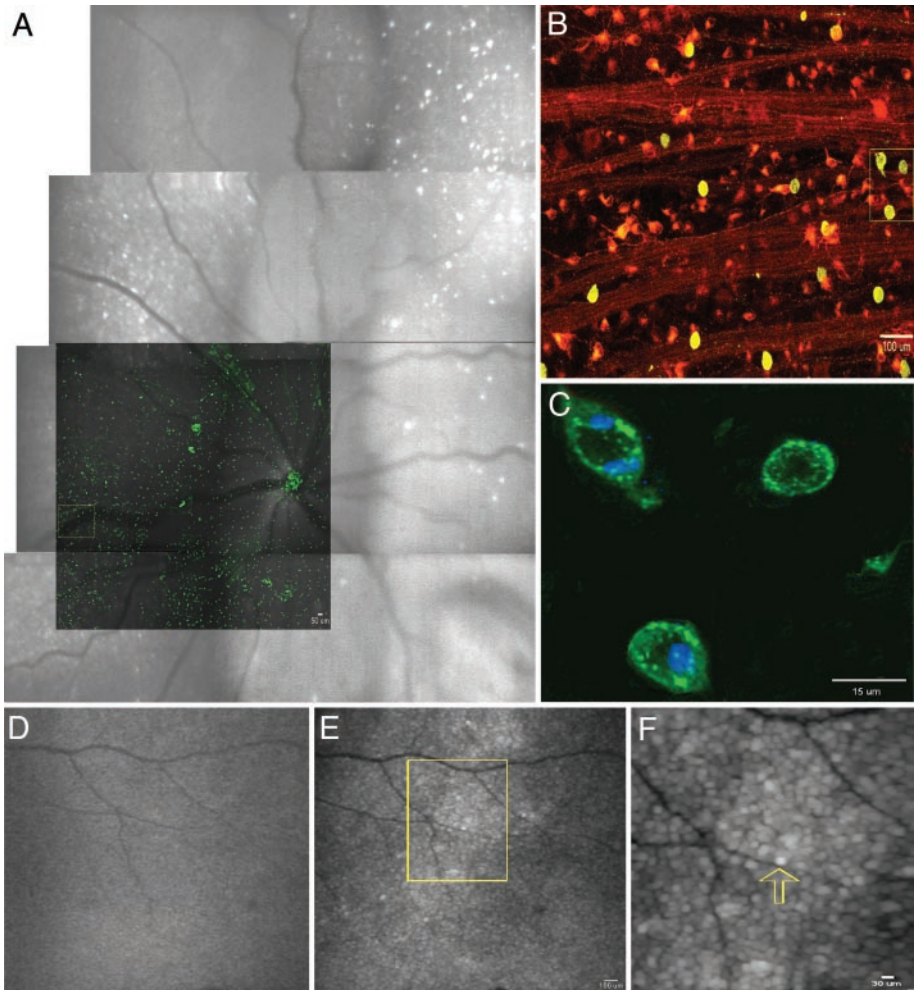

Fig. 2. Histological validation of nerve cell apoptosis. Anatomical reconstructions of *in vivo* and histological images revealed a good correlation of methods, with peak activity identified as occurring 3 weeks post-IOP elevation (*A*) and 7 days posttransection in rat models. (*A* and *B*; *A*, overlay of corresponding confocal microscopy over cLSO image, with magnified area *B*, respectively). RGC apoptosis (*A–C*, green, fluorescent-labeled annexin 5) was identified as occurring in individual RGCs retrogradely labeled with DiAsp (*B*, red staining) and confirmed histologically by double labeling of the same cells with annexin 5 and anti-caspase-3 (*C*, magnified area of *B*; blue, Cy5-labeled anti-caspase-3). Using intravitreal SSP in a primate model, we demonstrated direct visualization of single annexin 5-positive RGC (*D–F*). Baseline (*D*) and subsequent (*E* and *F*) cLSO *in vivo* images of the same area of primate retina 1 hr after 10-μg (high-dose) SSP injection showing widespread individual cellular RGC apoptosis [white staining, fluorescent-labeled annexin 5; *F*, magnified area of *E*; *F*, single cell (arrow)].

photodetector with a wide band-pass filter with a short-wavelength cutoff of a 521-nm filter. This signal was digitized by a frame grabber and stored on the computer. Sequences of raw images (typically 32–250) were automatically registered by the purposely written software to compensate for eye movements between images and then averaged to improve the signal to noise resulting in the two-dimensional images shown here.

For imaging, animals were held in a stereotaxic frame and their pupils dilated. Videos of scanned retinal areas were assessed for fluorescence as described (19). For each eye, a retinal montage was constructed from images captured at the same time point. All animals had baseline images recorded before receiving intravitreal injections of Alexa Fluor 488-labeled annexin 5. Pilot studies revealed the optimal doses to be 2.5 μg in 5 μl of PBS for the rat and 25 μg in 50 μl of PBS for the primate, with visualization of Alexa Fluor 488-labeled annexin 5 positivity up to 3 h after administration.

Histology. After killing, eyes were enucleated and fixed immediately in 4% fresh paraformaldehyde overnight, after which they were dissected at the equator, the lens and vitreous were removed, and whole flat retinas were obtained.

Apoptosis identification. For immunohistochemical identification of apoptotic populations, whole retinas were blocked [normal donkey serum, Jackson ImmunoResearch, 1:20 phosphate buffered Tween azide (PBTA)] for 2 h and then incubated with rabbit anti-active caspase-3 (BD Biosciences, Oxford, 1:300) at 4°C overnight, followed by incubation with donkey Cy5-conjugated anti-rabbit IgG (Jackson ImmunoResearch, 1:100 PBTA). After washing in PBS, the retinas were flattened by four radial cuts and mounted vitreal side up with Glycerol/PBS solution (Citifluor, Kent, U.K.).

Flat retinas were also processed for frozen section. Retinas were demounted, embedded in Tissue-Tek O.C.T (Sakura Finetechnical, Tokyo), and frozen in liquid nitrogen. The frozen retinal blocks were then cut into sections 7 μm in thickness and mounted in glycerol/PBS solution.

RGC identification. To identify RGCs unequivocally, a subgroup of rats had RGCs retrogradely labeled by the application of (4-(4-(didecylamino)styryl)-*N*-methylpyridinium iodide (DiAsp)

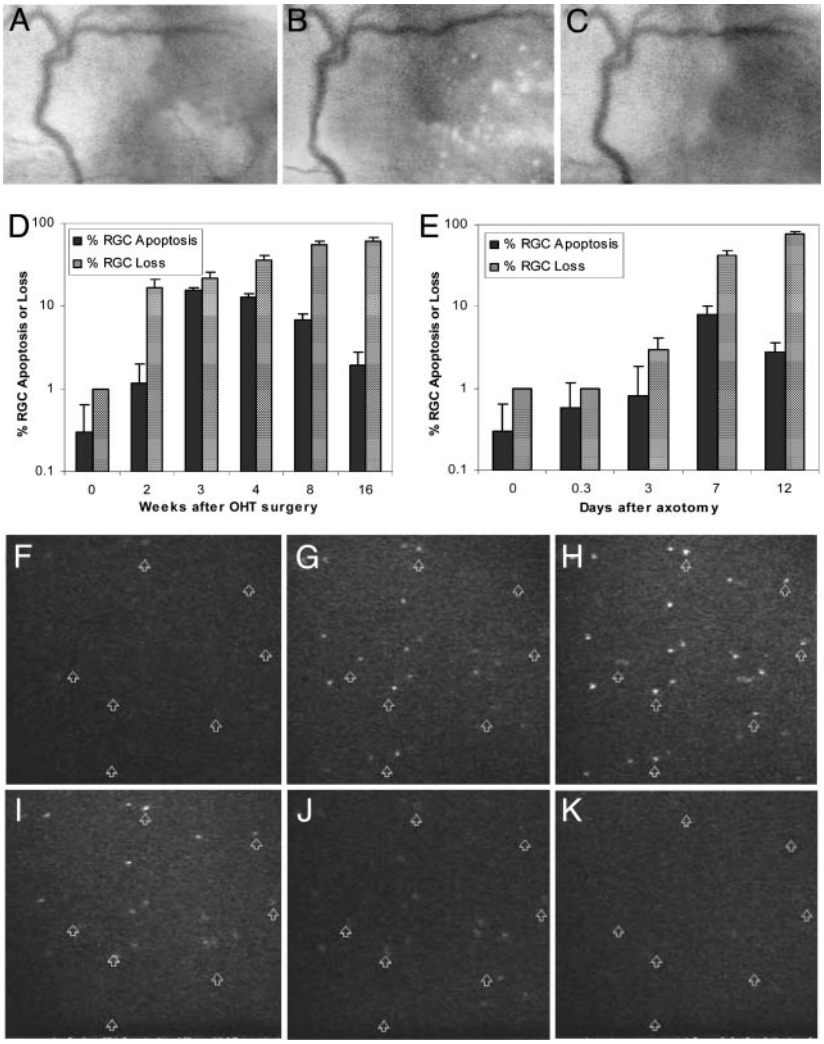

Fig. 3. RGC apoptosis changes recorded over time. Repeated imaging of the same OHT animal demonstrated differences in the RGC apoptotic profile over time at 2 (*A*), 4 (*B*), and 16 (*C*) weeks. We recorded a time-dependent effect in the rate of RGC apoptosis (RGC apoptosis as a percentage of total RGC count, identified histologically) in glaucoma (OHT) (*D*) and axotomized (*E*) rat eyes. Using our model of SSP-induced RGC apoptosis, we show time-lapse video sequences of the same scanned retinal areas in rat eyes (video, *F–K*). The appearance of different cells undergoing apoptosis (white spots, Alexa Fluor 488 fluorescence-labeled annexin 5) is seen within 10 min of each other at 80 (*F*), 90 (*G*), 100 (*H*), 110 (*I*), 120 (*J*), and 150 (*K*) minutes after 0.5 μg of intravitreal SSP. Individual cells (*F–K*) are indicated by arrows.

(4-Di-10-Asp, Molecular Probes) to both superior colliculi as described (20). These same rats underwent OHT surgery (n = 8) or axotomy (n = 6) 10 days later.

Whole flat retinas and frozen sections processed as described above were also stained with 4,6-diamidino-2-phenylindole (DAPI, Sigma–Aldrich, 1:2,500) to assess nuclei. This allowed the RGC layer to be identified anatomically in cross section.

Confocal microscopy. Fluorescent retinas were assessed by using a confocal laser scanning microscope (CLSM 510 META, Zeiss) with LSM software. This allowed detection of annexin 5, DiAsp, anti-caspase-3 (Cy-5), and 4,6-diamidino-2-phenylindole (DAPI). Using ×16 magnification, we assessed 81 adjacent microscopic fields (each measuring 0.329 mm^2) radiating outward from the optic nerve head in the rat and accounting for 40% of the whole retina. A retinal montage was then made for each whole retina.

Image analysis. The number of DiAsp-labeled RGC and annexin 5-labeled apoptotic RGCs was counted manually by using METAMORPH software (Universal Imaging, Downington, PA) by observers masked to treatment protocols. Statistical analysis was performed by using polynomial regression, Spearman's correlation, and ANOVA.

Results

Visualization of Single Nerve Cell Apoptosis *in Vivo*. Using a modified cLSO and intravitreal Alexa Fluor 488 fluorescent-labeled annexin 5, we investigated RGC apoptosis in rat models of OHT and optic nerve transection (axotomy). In addition, so that we could assess widespread apoptosis, we devised a model to generate rapid and extensive RGC apoptosis using intravitreal SSP, which is a nonselective protein kinase inhibitor and a well known potent inducer of neuronal apoptosis (21). We imaged OHT, axotomized and SSP-treated eyes at regular intervals after the administration of intravitreal fluorescent-labeled annexin 5 (2.5 μg), and demonstrated RGC apoptosis could be detected in all three models *in vivo* with this technique (Fig. 1).

Although real-time *in vivo* imaging of apoptosis with annexin 5 has been performed by using radiological-based techniques in structures other than the eye, these methods are unable to resolve the process to a cellular level. Instead, detection of apoptotic activity has been determined by the ability to pick up a signal from clusters of labeled cells in deeply lying internal organs, which cannot be directly visualized because of the relative opacity of the tissue (7–9). Our technique is unique because the optical properties of the eye allow direct observation and a microscopic approach to the detection of apoptosis as it occurs in single cells. Our *in vivo* findings were validated by histological assessment. We compared anatomical reconstructions of *in vivo* imaging with histological results of model eyes. These reconstructions revealed a good correlation of methods (Fig. 2*A*), with the demonstration of apoptosis, occurring in individual RGCs retrogradely labeled with DiAsp (Fig. 2*B*), confirmed by double-labeling of the same cells with annexin 5 and anti-caspase-3 (Fig. 2*C*).

Recording Changes in Nerve Cell Apoptosis Over Time. Due to the minimally invasive nature of our technique, we were able to assess the same animals at different time points. Imaging highlighted great differences in the amount of apoptosis demonstrated over time, with peak RGC apoptosis levels at 7 days in axotomy and 3–4 weeks in OHT models (Fig. 3 *A–C*). We demonstrated RGC apoptosis in OHT eyes as accounting for 1%, 15%, 13%, 7%, and 2% of total RGC, with RGC losses of 17%, 22%, 36%, 45%, and 60% of the original population at 2, 3, 4, 8, and 16 weeks, respectively (Fig. 3*D*). In axotomized eyes, we recorded apoptosis in 0.3%, 1%, 8%, and 3% of total RGCs, with RGC losses of 0%, 3%, 40%, and 76% at 0, 3, 7, and 12 days, respectively (Fig. 3*E*). Despite the fact that our measurement of RGC loss over time is similar to that of previous authors (22–26), we have recorded much higher rates of detection of RGC apoptosis (15, 23, 25). Compared with other methods such as DNA fragmentation, morphometry, time-lapse video microscopy, and microculture kinetic assays, annexin 5 has been shown to reveal apoptosis significantly earlier, with positive labeling of cells over a wide range of different stages of the apoptotic pathway (27).

Using time-lapse video sequences of the same scanned retinal

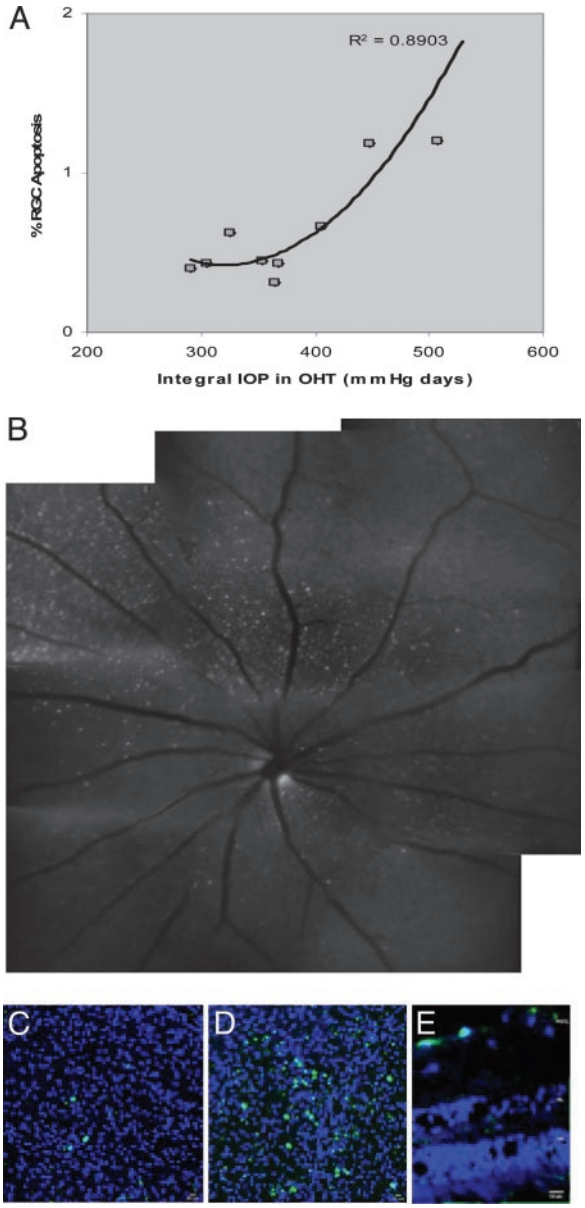

Fig. 4. RGC apoptosis depends on the magnitude of insult. Analysis of the effect of IOP on RGC apoptosis, using the parameter of ΔIOP integral as a measure of the cumulative effect of magnitude and duration of IOP elevation over time, demonstrated a significant positive correlation (polynomial regression, $r^2 = 0.89$, $P < 0.01$) with RGC apoptosis in glaucoma (OHT) rats studied until 8–16 weeks (*A*). SSP-induced RGC apoptosis demonstrated a clear dose-related effect both *in vivo* (*B*, cLSO images in rat, white staining, fluorescent-labeled annexin 5, 0.25 μg compared with Fig. 1, 0.5 μg of SSP) and histologically [*C–E*, confocal microscopy of primate eyes; whole retinal mounts (*C* and *D*) and frozen section (*E*); green, fluorescence-labeled annexin 5; blue, 4,6-diamidino-2-phenylindole (DAPI) nuclear stain]. Effects of SSP at doses of 5 (*C*) and 10 (*D* and *E*) μg are shown.

NEUROSCIENCE

areas in our intravitreal SSP-induced *in vivo* models, we showed a random distribution and appearance of apoptotic cells throughout the retina over the study period (see Movie 1, which is published as supporting information on the PNAS web site, and Fig. 3 *F–J*). The development of annexin 5 reactivity in our intravitreal SSP-induced *in vivo* model appears more rapid than *in vitro* studies of SSP, etoposide, and ricin, which have reported varying lag periods of 24 (21), 3–12 (27), and 3–4 h (28), respectively. Acquisition of annexin 5 positivity and eventual decay of the fluorescent signal occurred asynchronously across the retina, with evidence of the whole process in a single cell taking up to 3 h (Fig. 3 *F–J*). This finding is consistent with the morphological analysis of apoptosis *in vitro*, which suggests a 2- to 4-h period between the appearance of plasma membrane protrusions to the shedding of blebs of apoptotic cells (27–29). As far as we are aware, however, this is a previously undescribed demonstration of single nerve cell apoptosis *in vivo*.

RGC Apoptosis Depends on the Magnitude of Insult. Previous studies in glaucoma have suggested that RGC and axonal loss may be determined by the level of IOP elevation, (14, 22, 25, 30), with evidence that the extent of neuronal apoptosis induced *in vitro* is determined by the magnitude of the insult (21, 29). We next investigated the size of stimulus correlated with the level of apoptosis in our models. To assess the effect of IOP on RGC apoptosis, we used the parameter of ΔIOP integral as a measure of the cumulative effect of magnitude and duration of IOP and demonstrated a significant positive correlation with RGC apoptosis in OHT rats studied at 8–16 weeks (Fig. 4*A*). This has not previously been assessed. In addition, we found that SSP-induced RGC apoptosis demonstrated a clear dose-dependent effect in rat (Figs. 1 and 4*B*) and primate (Fig. 4 *C–E*) models, both *in vivo* and histologically, with toxic lens epithelial effects precluding *in vivo* imaging in the rat beyond 0.5 μg.

Discussion

This is the first time, to our knowledge, that neuronal apoptosis in the eye of a living animal has been observed. Unlike previous reports, we have been able to visualize individual and single cells apoptosing in real time (7–9) with a minimally invasive (10) procedure that utilizes the unique optical properties of the eye. The retina as a window on the brain may also enable this procedure to highlight possible links to other neural degenerative diseases that may include a parallel damage to RGCs.

Annexin 5 detects apoptosis significantly earlier than other methods (27). Its binding to the apoptotic cell membrane (phosphotidyl serine) is linked to key steps in the apoptotic process, particularly activation of caspase 3. This has great implications for our technique being used to assess potential therapies preventing early apoptosis, e.g., caspase inhibitors (31). In addition, because binding of annexin 5 continues for >24 h after initiation of apoptosis (27), our ability to observe changes in individual cells over time would facilitate comparisons of strategies targeting different components of the apoptotic pathway, right up to the final end point of cell death.

Our technique opens up the possibility for the investigation of nerve cell apoptosis in the same animal over a period of hours, days, weeks, or even longer, and to observe the normal time course of apoptosis during development, discover spatial patterns in the evolution of apoptosis, and understand how apoptosis may be modulated by environmental factors or pharmacological inhibitors. Because the cellular responses to potential modulators of apoptosis may vary with their environment, this would allow an understanding of how apoptosis is modulated in the living animal and more directly lead to determining the therapeutic potential of inhibitors. It opens the door to the possibility of making this type of observation in the retina of patients with retinal disease.

We thank Annelie Maass for technical assistance; Carl Zeiss for donating the prototype cLSO; and the Wellcome Trust, the Foundation Fighting Blindness, and Allergan, Incorporated, for support.

1. Vila, M. & Przedborski, S. (2003) *Nat. Rev. Neurosci.* **4,** 365–375.
2. McKinnon, S. J., Lehman, D. M., Kerrigan-Baumrind, L. A., Merges, C. A., Pease, M. E., Kerrigan, D. F., Ransom, N. L., Tahzib, N. G., Reitsamer, H. A., Levkovitch-Verbin, H., *et al.* (2002) *Invest. Ophthalmol. Visual Sci.* **43,** 1077–1087.
3. Auld, D. S., Kornecook, T. J., Bastianetto, S. & Quirion, R. (2002) *Prog. Neurobiol.* **68,** 209–245.
4. Nakamura, S., Murayama, N., Noshita, T., Annoura, H. & Ohno, T. (2001) *Brain Res.* **912,** 128–136.
5. Kerrigan-Baumrind, L., Quigley, H., Pease, M., Kerrigan, D. & Mitchell, R. (2000) *Invest. Ophthalmol. Visual Sci.* **41,** 741–748.
6. Harwerth, R., Carter-Dawson, L., Shen, F., Smith, E. & Crawford, M. (1999) *Invest. Ophthalmol. Visual Sci.* **40,** 2242–2250.
7. Zhao, M., Beauregard, D. A., Loizou, L., Davletov, B. & Brindle, K. M. (2001) *Nat. Med.* **7,** 1241–1244.
8. Laxman, B., Hall, D. E., Bhojani, M. S., Hamstra, D. A., Chenevert, T. L., Ross, B. D. & Rehemtulla, A. (2002) *Proc. Natl. Acad. Sci. USA* **99,** 16551–16555.
9. Reutelingsperger, C. P., Dumont, E., Thimister, P. W., van Genderen, H., Kenis, H., van de Eijnde, S., Heidendal, G. & Hofstra, L. (2002) *J. Immunol. Methods* **265,** 123–132.
10. Dumont, E. A., Reutelingsperger, C. P., Smits, J. F., Daemen, M. J., Doevendans, P. A., Wellens, H. J. & Hofstra, L. (2001) *Nat. Med.* **7,** 1352–1355.
11. Vermes, I., Haanen, C., Steffens-Nakken, H. & Reutelingsperger, C. (1995) *J. Immunol. Methods* **184,** 39–51.
12. Narula, J., Acio, E. R., Narula, N., Samuels, L. E., Fyfe, B., Wood, D., Fitzpatrick, J. M., Raghunath, P. N., Tomaszewski, J. E., Kelly, C., *et al.* (2001) *Nat. Med.* **7,** 1347–1352.
13. Blankenberg, F. G. & Strauss, H. W. (2001) *Apoptosis* **6,** 117–123.
14. Morrison, J. C., Moore, C. G., Deppmeier, L. M., Gold, B. G., Meshul, C. K. & Johnson, E. C. (1997) *Exp. Eye Res.* **64,** 85–96.
15. Mo, X., Yokoyama, A., Oshitari, T., Negishi, H., Dezawa, M., Mizota, A. & Adachi-Usami, E. (2002) *Invest. Ophthalmol. Visual Sci.* **43,** 2401–2405.
16. Jones, H. E., Grieve, K. L., Wang, W. & Sillito, A. M. (2001) *J. Neurophysiol.* **86,** 2011–2028.
17. Wade, A. R. & Fitzke, F. W. (1998) *Optics Express* **3,** 190–197.
18. von Ruckmann, A., Fitzke, F. W. & Bird, A. C. (1995) *Br. J. Ophthalmol.* **79,** 407–412.
19. Fitzke, F. (2000) *Eye* **14,** 450–453.
20. Naskar, R., Wissing, M. & Thanos, S. (2002) *Invest. Ophthalmol. Visual Sci.* **43,** 2962–2968.
21. Koh, J. Y., Wie, M. B., Gwag, B. J., Sensi, S. L., Canzoniero, L. M., Demaro, J., Csernansky, C. & Choi, D. W. (1995) *Exp. Neurol.* **135,** 153–159.
22. Levkovitch-Verbin, H., Quigley, H. A., Martin, K. R., Valenta, D., Baumrind, L. A. & Pease, M. E. (2002) *Invest. Ophthalmol. Visual Sci.* **43,** 402–410.
23. Quigley, H. A., Nickells, R. W., Kerrigan, L. A., Pease, M. E., Thibault, D. J. & Zack, D. J. (1995) *Invest. Ophthalmol. Visual Sci.* **36,** 774–786.
24. Mittag, T. W., Danias, J., Pohorenec, G., Yuan, H. M., Burakgazi, E., Chalmers-Redman, R., Podos, S. M. & Tatton, W. G. (2000) *Invest. Ophthalmol. Visual Sci.* **41,** 3451–3459.
25. Garcia-Valenzuela, E., Shareef, S., Walsh, J. & Sharma, S. C. (1995) *Exp. Eye Res.* **61,** 33–44.
26. WoldeMussie, E., Ruiz, G., Wijono, M. & Wheeler, L. A. (2001) *Invest. Ophthalmol. Visual Sci.* **42,** 2849–2855.
27. Kravtsov, V. D., Daniel, T. O. & Koury, M. J. (1999) *Am. J. Pathol.* **155,** 1327–1339.
28. Collins, J. A., Schandi, C. A., Young, K. K., Vesely, J. & Willingham, M. C. (1997) *J. Histochem. Cytochem.* **45,** 923–934.
29. Deckwerth, T. L. & Johnson, E. M., Jr. (1993) *J. Cell Biol.* **123,** 1207–1222.
30. Agar, A., Yip, S. S., Hill, M. A. & Coroneo, M. T. (2000) *J. Neurosci. Res.* **60,** 495–503.
31. Garg, S., Hofstra, L., Reutelingsperger, C. & Narula, J. (2003) *Curr. Opin. Cardiol.* **18,** 372–377.